Missile Autopilot Design Via Functional Inversion and Time-Scaled Transformation

JAE-HYUK OH
IN-JOONG HA
Seoul National University

This paper presents a new approach to acceleration control of STT (Skid-To-Turn) missiles. In the design and stability analysis of our autopilot, we assume perfect roll-stabilization but consider fully all other nonlinearities of the missile dynamics including the coupling effect due to bank angle. Our autopilot controller consists of a partial-linearizing controller and a dynamic compensator. The partial-linearizing controller along with a time-scaled transformation can convert the nonlinear missile dynamics to the so-called normalized system which is completely independent of Mach number and almost independent of air density. The dynamic compensator is designed based on this normalized system. This normalized system greatly simplifies the design process of an autopilot controller regardless of flight conditions. Our autopilot controller can provide fast and exact set-point tracking performance but without the slow-varying conditions on angle of attack and side-slip angle required often in the prior works.

Manuscript received July 14, 1994; revised July 14, 1995.

IEEE Log No. T-AES/33/1/01075.

Authors' address: Dept. of Control and Instrumentation Engineering, Automatic Control Research Center, Seoul National University, San 56-1 Shinrim-Dong, Kwanak-Ku, Seoul 151-742, Korea.

I. NOMENCLATURE

(X,Y,Z)	Missile body coordinate system
i,j,k	Unit vectors along the X-, Y-, Z-axes, respectively
U,V,W	X-, Y-, Z-components, respectively, of the linear velocity vector of the missile
p,q,r	X-, Y-, Z-components, respectively, of the angular velocity vector of the missile
I_y,I_z	Moments of inertia about Y-, Z-axes, respectively
I_{xy},I_{yz},I_{zx}	Products of inertia
V_S	Velocity of sound
V_M	Total velocity of the missile ($\triangleq \sqrt{\lvert U\rvert^2+\lvert V\rvert^2+\lvert W\rvert^2}$)
M	Mach number ($\triangleq V_M/V_S$)
γ	Total angle ($\triangleq \tan^{-1}(\sqrt{\lvert V\rvert^2+\lvert W\rvert^2}/V_M)$)
α,β,ϕ	Angle of attack, side-slip angle, bank angle ($\alpha \triangleq \tan^{-1}(W/U)$, $\beta \triangleq \tan^{-1}(V/U)$, $\phi \triangleq \tan^{-1}(W/V)$)
m	Missile mass
ρ	Air density
Q	Dynamic pressure ($\triangleq \rho\lvert V_M\rvert^2/2$)
S	Aerodynamic reference area
D	Aerodynamic reference length
$\delta_r(\delta_q)$	Deflection of yaw (pitch) control fin
$\delta_r^c(\delta_q^c)$	Yaw (pitch) control fin command
$A_y(A_z)$	Yaw (pitch) acceleration of the missile
$A_y^c(A_z^c)$	Yaw (pitch) acceleration command
$F_y(F_z)$	Y- (Z-) component of the total aerodynamic force vector
$M_y(M_z)$	Y- (Z-) component of the total aerodynamic moment vector
$H_y(H_z)$	Lateral (normal) force coefficient
$H_m(H_n)$	Pitching (yawing) moment coefficient
$\lvert x\rvert$	Euclidean norm of a vector $x \in \Re^n$
$D_i f(x_1,\ldots,x_n)$	Partial derivative at the point $(x_1,\ldots,x_n) \in \Re^n$ of $f : \Re^n \to \Re$ with respect to the ith argument
$\mathcal{L}[f(t)]$	Laplace transform of a function $f : [0,\infty) \to \Re$
I_{V_M}	Range of total velocity V_M ($\triangleq [V_{M\min}, V_{M\max}]$)
I_ρ	Range of air density ρ ($\triangleq [\rho_{\min},\rho_{\max}]$)
I_δ	Range of control fin deflections δ_r,δ_q
S_{VW}	Range of V/V_M and W/V_M such that $\gamma \le \gamma_{\max}$ ($\triangleq \{(x,y) \in \Re^2 : \lvert x\rvert^2+\lvert y\rvert^2 \le \sin^2\gamma_{\max}\}$).

II. INTRODUCTION

We consider the autopilot design for short-range surface-to-air STT (Skid-to-Turn) missiles. Although the BTT (Bank-to-Turn) technique for high maneuverability is best matched to ramjet engines for high fuel efficiency, the STT technique is still dominantly employed in both surface-to-air and air-to-air missile applications [1]. This is mainly because the STT technique can make inertial cross coupling between roll, pitch, and yaw dynamics negligible. However, the bank angle still causes coupling between the pitch and yaw dynamics and can vary largely even in a short period in case of high maneuvering. Also, both aerodynamics and rigid-body-dynamics of STT missiles are still highly nonlinear. Moreover, the aerodynamics cannot be described in closed form but is available only in look-up table form. All of these facts make it still difficult to design a high performance autopilot for STT missiles.

The autopilot designed via the well-known linear perturbation technique usually can give the desired performance only in case of small missile acceleration or small angle of attack. Moreover, the autopilot performance depends on the equilibrium points or flight conditions. Recently, a lot of effort has been made in finding more effective design methods for missile autopilot. In [2], a kind of "partial" pseudolinearization technique is proposed to reduce the effect of flight conditions on the autopilot performance since direct application of the usual pseudolinearization technique [3] leads to unstable pole-zero cancellation. In [4, 5], the so-called gain-scheduling approach is taken to the design of missile autopilot in order to make the desired performance specifications satisfied regardless of equilibrium points. In [4], the well-known H^∞ control method is incorporated into the gain-scheduling approach in order to simplify the gain-scheduling procedure. This gain-scheduling approach can be justified rigorously under some slow-varying conditions on Mach number, angle of attack, and side-slip angle used as scheduling variables [6]. In [5], a new gain-scheduling approach is proposed in order to relax the slow-varying condition on angle of attack. It is based on a family of linear systems with angle of attack as an exogenous time-varying parameter, which are obtained via a state transformation but not from the usual linear perturbation technique.

On the other hand, the well-known I/O (input/output) feedback linearization technique [7] is to linearize I/O dynamic characteristics of nonlinear systems via feedback and takes system nonlinearities directly and fully into account. In fact, it has been successfully applied not only to derivation of an exact CLOS (command to the line-of-sight) guidance law for surface-to-air missiles [8] but also to autopilot design for helicopters [9], aircrafts [10], and BTT missiles [11]. Unfortunately, direct applications of I/O feedback linearization technique to flight vehicles often involve differentiation of uncertain aerodynamic functions. In reality, this may degrade autopilot performance significantly. In [11], a robust feedback linearization approach is proposed to overcome this drawback. However, such successful applications of feedback linearization technique were possible because the outputs to be controlled are not acceleration but other variables such as angular position or angle of attack. In fact, the direct application of I/O feedback linearization technique to acceleration control of missiles cannot guarantee internal stability since it can leave the hidden or zero dynamics unstable. See [12] for the details of other prior works on missile autopilot design.

We propose a new approach to acceleration control of STT missiles, which can handle effectively the nonlinearities of missile dynamics. First, we transform the nonlinear missile dynamics into an "almost-linear" system via a kind of functional inversion technique utilizing the fact that one component of the aerodynamic force is invertible with respect to control fins. By an almost-linear system, we mean a system which has a linear system in feedfoward path and a memoryless nonlinearity in feedback path. Using a time-scaled transformation and a dynamic compensator, we then convert the almost-linear system to a normalized system which is completely independent of Mach number and almost independent of air density.

The partial linearization technique introduced in [13, 14] is to transform a nonlinear system via state feedback into a system consisting of a linear main system and a nonlinear subsystem. In this context, it is conceptually similar to our functional inversion technique and the I/O feedback linearization technique mentioned above also may be viewed as a kind of partial linearization technique. However, the partial linearization technique concerns a class of nonlinear systems without the output, which does not include the nonlinear dynamics of STT missiles.

Our approach can remove some drawbacks of the previously known design methods effectively. First, we can completely remove the slow-varying conditions on angle of attack and side-slip angle required for stability in the prior works. Only Mach number and air density which vary slowly compared with the autopilot bandwidth are used as the scheduling variables for our autopilot controller. As the result, our approach to acceleration control of STT missiles can provide very fast transient responses to acceleration commands. Second, our normalized system can facilitate greatly the scheduling procedure with respect to Mach number and air density. Note that, in the prior works, air density is assumed to be constant. Third, our autopilot design method does not involve differentiation of uncertain aerodynamic functions and

produces no unstable hidden dynamics. Fourth, we present a rigorous stability analysis of our autopilot controller, which considers all other nonlinearities of missile dynamics including the coupling effect due to bank angle, although perfect roll-stabilization is assumed. Finally, we emphasize that the missile model considered here is quite more general than those considered in the prior literature.

III. PRELIMINARIES

We make the following assumptions in deriving a dynamic model for short-range surface-to-air STT Missiles.

A1. m, I_y, and I_z are constant.
A2. V_S, ρ, and V_M are constant.
A3. Missile is of Y and Z symmetry.
A4. Missile is roll-stabilized.
A5. $U = V_M$.

The assumptions A1–A4 are commonly accepted for a short-range STT missile in flight with its thrust burn out. It can be easily shown that $0.9V_M \le U \le V_M$ if $\gamma \le 25°$. On the other hand, the total angle of a STT missile hardly can exceed 25° even in case of very high maneuvering. Hence, A5 is also a reasonable assumption. By A1, A3, and A4, we let

$$I_y = I_z = I_M, \qquad I_{xy} = I_{yz} = I_{zx} = 0, \qquad p = 0 \tag{1}$$

where $I_M > 0$ is a constant.

Under these assumptions, we can describe the 3-dimensional motion of a STT missile by the following set of nonlinear ordinary differential equations:

$$\text{yaw channel} \quad \begin{cases} \dot{V} = -V_M r + \dfrac{QS}{m} H_y(V, W, \delta_r, V_M) \\ \dot{r} = \dfrac{QSD}{I_M} H_n(V, W, \delta_r, V_M) \\ A_y = \dfrac{QS}{m} H_y(V, W, \delta_r, V_M) \end{cases} \tag{2a}$$

$$\text{pitch channel} \quad \begin{cases} \dot{W} = V_M q + \dfrac{QS}{m} H_z(V, W, \delta_q, V_M) \\ \dot{q} = \dfrac{QSD}{I_M} H_m(V, W, \delta_q, V_M) \\ A_z = \dfrac{QS}{m} H_z(V, W, \delta_q, V_M) \end{cases} . \tag{2b}$$

In most cases, the aerodynamic coefficients H_y, H_n, H_z, and H_m in (2) are obtained in look-up table form through wind-tunnel experiments and are represented in terms of α, β, ϕ, M, and deflections of control fins. Nonetheless, we prefer to write the dynamic equations of missile motion in terms of V, W, and V_M rather than α, β, ϕ, and M. As seen sooner or later, the choice of V and W as state variables facilitates greatly our autopilot design method presented in the next section. In modeling, we have neglected the coupling effect of δ_q and δ_r since it is expected to be negligible in the ideal case when the force acting on a flying plate is normal to that plate. The damping effect also has been eliminated from the moment equations in (2) since it is insignificant.

Note from (2) that the pitch and yaw channels are still aerodynamically coupled, although they are not subject to inertial cross coupling. In most prior works on control of STT missiles, it is assumed that ϕ is sufficiently small or slowly varying and, hence, that the pitch and yaw channels are decoupled. Here, we emphasize that the aerodynamic coupling between the two channels as well as the nonlinearities of missile dynamics is taken into full account in our autopilot design.

The missile model in (2) is not yet useful for autopilot design since it does not specify the detailed structure of the functions H_y, H_n, H_z, and H_m. For this reason, we now attempt to characterize the properties of these functions, which are useful for our autopilot design. To do so, we need to make three other assumptions on the aerodynamic characteristics of STT missiles. Let $F_M \triangleq F_x i + F_y j + F_z k$ be the total aerodynamic force acting on the missile. Let $F_B \triangleq F_{Bx} i + F_{By} j + F_{Bz} k$ be the force which is generated by the cylindrical body of the missile. Let $F_C \triangleq F_{Cx} i + F_{Cy} j + F_{Cz} k$ be the force which is generated by the control fins of the missile. We denote the normal components of F_B and F_C by $F_{B_N} \triangleq F_{By} j + F_{Bz} k$ and $F_{C_N} \triangleq F_{Cy} j + F_{Cz} k$, respectively. Finally, let l_g, l_b, and l_f denote the distances from the nose of the missile to the center-of-gravity, the center-of-pressure of cylindrical body, and the center-of-pressure of control fins, respectively.

Then, the following assumption is quite reasonable [1].

A6. F_y, F_z, M_y, and M_z are decomposed as follows:

$$F_y = F_{By} + F_{Cy}, \qquad F_z = F_{Bz} + F_{Cz} \tag{3a}$$

$$\begin{aligned} M_y &= (l_b - l_g) F_{Bz} + (l_f - l_g) F_{Cz}, \\ M_z &= -(l_b - l_g) F_{By} - (l_f - l_g) F_{Cy}. \end{aligned} \tag{3b}$$

In other words, we assume that F_y and F_z can be decomposed of one component which depends on control fins and the other component which does not. We also assume that M_y and M_z can be determined completely by the normal components of F_B and F_C. Unfortunately, we cannot express F_{C_N} in a closed form because it depends in a highly complicated fashion on deflections of control fins. Nonetheless, most missiles are supposed to satisfy the next assumption.

A7. F_{Cy} and F_{Cz} are strictly increasing in δ_r and δ_q, respectively.

In fact, existing nonlinear missile models [4, 5, 11, 12] consider F_{C_N} to be nearly linear about deflections of control fins. The final assumption we make is as follows.

A8. F_{B_N} depends only on Q and γ such that

$$|F_{B_N}| = Q f_N(\gamma) \tag{4}$$

where the function $f_N : [0^\circ, \gamma_{\max}] \to \Re$ is continuously differentiable and is strictly increasing in γ.

Strictly speaking, f_N depends on ϕ and V_M as well as γ. Nonetheless, the effect of ϕ and V_M are known to be relatively negligible when $\gamma \le 25^\circ$ and $V_M \ge V_S$. In fact, Morton [15] has shown on the basis of experimental data that f_N can be simply represented by $f_N(\gamma) = k\sin(\gamma)$, $k > 0$, which obviously satisfies the assumption A8 with $\gamma_{\max} < 45^\circ$.

Now, we are ready to characterize some properties of H_y, H_z, H_m, and H_n which appear in our missile model in (2). Define the functions H_a and H_b as follows:

$$H_a(\hat{V},\hat{W}) \triangleq \begin{cases} 0, & \text{if} \quad \hat{V} = \hat{W} = 0 \\ \left(\dfrac{l_f - l_b}{I_M}\right) \dfrac{\hat{V}}{\sqrt{|\hat{V}|^2 + |\hat{W}|^2}} f_N\left(\sin^{-1}\left(\sqrt{|\hat{V}|^2 + |\hat{W}|^2}\right)\right), & \text{otherwise} \end{cases} \tag{5a}$$

$$H_b(\hat{V},\hat{W}) \triangleq \begin{cases} 0, & \text{if} \quad \hat{V} = \hat{W} = 0 \\ \left(\dfrac{l_f - l_b}{I_M}\right) \dfrac{\hat{W}}{\sqrt{|\hat{V}|^2 + |\hat{W}|^2}} f_N\left(\sin^{-1}\left(\sqrt{|\hat{V}|^2 + |\hat{W}|^2}\right)\right), & \text{otherwise} \end{cases} \tag{5b}$$

By the definitions of F_{By}, F_{Bz}, H_a, and H_b along with A8, we then have the following relationships:

$$F_{By} = -|F_{B_N}|\cos\phi = \frac{QI_M}{l_b - l_f} H_a\left(\frac{V}{V_M}, \frac{W}{V_M}\right) \tag{6a}$$

$$F_{Bz} = -|F_{B_N}|\sin\phi = \frac{QI_M}{l_b - l_f} H_b\left(\frac{V}{V_M}, \frac{W}{V_M}\right). \tag{6b}$$

Thus, the functions H_a and H_b describe how the forces F_{By} and F_{Bz} depend on V, W, and V_M. In particular, (6) shows that F_{By} and F_{Bz} depend on the normalized variables V/V_M and W/V_M rather than individually on each of V, W, and V_M.

Let $(\hat{V}^*, \hat{W}^*) \in S_{VW}$. And define $\tilde{V} \triangleq \hat{V} - \hat{V}^*$, $\tilde{W} \triangleq \hat{W} - \hat{W}^*$, and

$$\tilde{H}_a(\tilde{V},\tilde{W},\hat{V}^*,\hat{W}^*) \triangleq H_a(\tilde{V}+\hat{V}^*,\tilde{W}+\hat{W}^*) - H_a(\hat{V}^*,\hat{W}^*) \tag{7a}$$

$$\tilde{H}_b(\tilde{V},\tilde{W},\hat{V}^*,\hat{W}^*) \triangleq H_b(\tilde{V}+\hat{V}^*,\tilde{W}+\hat{W}^*) - H_b(\hat{V}^*,\hat{W}^*). \tag{7b}$$

That is, $\tilde{H}_a$, $\tilde{H}_b$ are the perturbed functions of H_a, H_b, respectively, around an equilibrium point $(\hat{V}^*, \hat{W}^*)$. Then, the following lemma shows that the nonlinear functions H_a and H_b satisfy a sector condition for vector nonlinearities [16] if A8 holds.

LEMMA 1 *If* A8 *holds, there exist positive constants* k_1, k_2, k_3 *such that*

$$\begin{aligned} &\left\{\tilde{H}_a - (k_1 + k_3)\tilde{V}\right\}\left\{\tilde{H}_a - (k_2 - k_3)\tilde{V}\right\} \\ &\quad + \left\{\tilde{H}_b - (k_1 + k_3)\tilde{W}\right\}\left\{\tilde{H}_b - (k_2 - k_3)\tilde{W}\right\} \le 0, \\ &\quad \text{for all} \quad (\hat{V},\hat{W}), \quad (\hat{V}^*,\hat{W}^*) \quad \text{in} \quad S_{VW}. \end{aligned} \tag{8}$$

PROOF By A8 and (5), it is obvious that the functions H_a and H_b are continuously differentiable at each point in the set S_{VW}. Moreover, S_{VW} is a compact subset of $\Re^2$. Therefore, there exist the minima and maxima of the partial derivatives D_1H_a, D_2H_a, D_1H_b, and D_2H_b on S_{VW}. On the other hand, direct calculations with the aid of A8 show that D_1H_a and D_2H_b are always positive on S_{VW}. Consequently, there exist positive constants k_1, k_2, k_3 such that,

$\forall (\hat{V},\hat{W}) \in S_{VW}$,

$$\begin{aligned} k_2 \le D_1H_a(\hat{V},\hat{W}) \le k_1, \\ |D_2H_a(\hat{V},\hat{W})| \le k_3 \end{aligned} \tag{9a}$$

$$\begin{aligned} k_2 \le D_2H_b(\hat{V},\hat{W}) \le k_1, \\ |D_1H_b(\hat{V},\hat{W})| \le k_3. \end{aligned} \tag{9b}$$

By these inequalities and *Mean-Value Theorem for derivatives* [17], we then have the following inequalities:

$$\begin{aligned} f_L \le \tilde{H}_a \le f_U, \\ g_L \le \tilde{H}_b \le g_U, \end{aligned} \quad \forall \quad (\hat{V},\hat{W}), \quad (\hat{V}^*,\hat{W}^*) \in S_{VW} \tag{10}$$

where

$$\begin{aligned} f_L &\triangleq k_2\tilde{V} - k_3|\tilde{W}|, & f_U &\triangleq k_1\tilde{V} + k_3|\tilde{W}| \\ g_L &\triangleq k_2\tilde{W} - k_3|\tilde{V}|, & g_U &\triangleq k_1\tilde{W} + k_3|\tilde{V}|. \end{aligned} \tag{11}$$

Also, note that $2|\tilde{V}\tilde{W}| \le |\tilde{V}|^2 + |\tilde{W}|^2$ and $(k_1 - k_2)k_3 \ge 0$. By this with (10) and (11), we finally have

$$
\begin{aligned}
0 &\geq (\tilde{H}_a - f_L)(\tilde{H}_a - f_U) + (\tilde{H}_b - g_L)(\tilde{H}_b - g_U) \\
&\geq |\tilde{H}_a|^2 + |\tilde{H}_b|^2 - (k_1 + k_2)\tilde{V}\tilde{H}_a - (k_1 + k_2)\tilde{W}\tilde{H}_b \\
&\quad + (k_1 k_2 - |k_3|^2)(|\tilde{V}|^2 + |\tilde{W}|^2) - 2(k_1 - k_2)k_3|\tilde{V}\tilde{W}| \\
&\geq |\tilde{H}_a|^2 + |\tilde{H}_b|^2 - (k_1 + k_2)(\tilde{V}\tilde{H}_a + \tilde{W}\tilde{H}_b) \\
&\quad + (k_2 - k_3)(k_1 + k_3)(|\tilde{V}|^2 + |\tilde{W}|^2) \\
&\quad \forall \quad (\hat{V}, \hat{W}), \quad (\hat{V}^*, \hat{W}^*) \in S_{VW}. \qquad (12)
\end{aligned}
$$

Now, the inequality in (8) is the immediate consequence of the above one. □

The above lemma is used in showing the stability of our autopilot proposed in the next section by using the well-known *Multivariable Circle Criterion Theorem* [16]. In the proof of the above lemma, we have shown that the inequalities in (9) imply that in (8). It should be noted that the former can be verified, in practice, much more easily than the latter. Therefore, we had better calculate the partial derivatives of H_a and H_b numerically by using aerodata given in a look-up table form and then choose the constants k_1, k_2, k_3 so as to satisfy the inequalities in (9).

Finally, note that

$$
\begin{aligned}
F_y &= QSH_y(V, W, \delta_r, V_M), \\
F_z &= QSH_z(V, W, \delta_q, V_M)
\end{aligned} \qquad (13a)
$$

$$
\begin{aligned}
M_y &= QSDH_m(V, W, \delta_q, V_M), \\
M_z &= QSDH_n(V, W, \delta_r, V_M).
\end{aligned} \qquad (13b)
$$

From (6) and (13) along with A6, we then can find that the following relationships hold between the functions H_m, H_n, H_y, H_z, H_a, and H_b:

$$
\begin{aligned}
H_m(V, W, \delta_q, V_M) &= \frac{I_M}{SD} H_b\left(\frac{V}{V_M}, \frac{W}{V_M}\right) \\
&\quad + \frac{l_f - l_g}{D} H_z(V, W, \delta_q, V_M)
\end{aligned} \qquad (14a)
$$

$$
\begin{aligned}
H_n(V, W, \delta_r, V_M) &= -\frac{I_M}{SD} H_a\left(\frac{V}{V_M}, \frac{W}{V_M}\right) \\
&\quad - \frac{l_f - l_g}{D} H_y(V, W, \delta_r, V_M).
\end{aligned} \qquad (14b)
$$

As can be seen in the next section, our functional inversion technique transforms the nonlinear missile model into an almost-linear system by utilizing the above facts.

V. MAIN RESULTS

In this section, we describe our approach to the autopilot design for STT missiles. In design process, we neglect actuator dynamics. That is, we assume that $\delta_r = \delta_r^c$ and $\delta_q = \delta_q^c$. Nonetheless, we show through simulation that the effect of actuator dynamics on the performance of our autopilot is not significant.

It is clear from A7 that H_y and H_z are invertible. Hence, there exist the mappings K_y and K_z satisfying

$$
H_y(V, W, K_y(V, W, u_y, V_M), V_M) = u_y \qquad (15a)
$$

$$
H_z(V, W, K_z(V, W, u_z, V_M), V_M) = u_z. \qquad (15b)
$$

Now, choose the control fin commands δ_r^c and δ_q^c by

$$
\delta_r^c \triangleq K_y\left(V, W, \frac{m(v_y + V_M r)}{QS}, V_M\right) \qquad (16a)
$$

$$
\delta_q^c \triangleq K_z\left(V, W, \frac{m(v_z - V_M q)}{QS}, V_M\right) \qquad (16b)
$$

where v_y and v_z are the new inputs. By (14) and (15), we then see that the control fin commands δ_r^c, δ_q^c given by (16) take the missile model in (2) to the almost-linear system as follows:

$$
\text{yaw channel} \quad \begin{cases} \dot{V} = v_y \\ \dot{r} = -QH_a\left(\dfrac{V}{V_M}, \dfrac{W}{V_M}\right) - h_v v_y - h_v V_M r \\ A_y = v_y + V_M r \end{cases} \qquad (17a)
$$

$$
\text{pitch channel} \quad \begin{cases} \dot{W} = v_z \\ \dot{q} = QH_b\left(\dfrac{V}{V_M}, \dfrac{W}{V_M}\right) + h_v v_z - h_v V_M q \\ A_z = v_z - V_M q \end{cases} \qquad (17b)
$$

where

$$
h_v \triangleq \frac{(l_f - l_g)m}{I_M}. \qquad (17c)
$$

Note that the functions H_a and H_b can be viewed as the mathematical representations of some memoryless nonlinear elements. From (17), we see that the controller in (16) partial-linearizes the nonlinear system in (2). In this sense, we call it a partial-linearizing controller from now on. This partial linearization facilitates autopilot design since the resulting system in (17) is almost linear and its nonlinearities can be characterized quantitatively well by Lemma 1 in the previous section.

Note, however, that the partial-linearized system in (17) has V_M and ρ as system parameters. Accordingly, we have to consider simultaneously a family of nonlinear systems indexed by V_M and ρ. However, this makes it difficult to design an autopilot which can satisfy, regardless of V_M and ρ, various performance specifications including stability. To overcome this difficulty, we now introduce what we call time-scaled transformation.

Define the new inputs $\hat{v}_y$, $\hat{v}_z$, the new outputs $\hat{A}_y$, $\hat{A}_z$, and the new state variables $\hat{V}$, $\hat{W}$, $\hat{r}$, $\hat{q}$ by

$$\hat{v}_y(t) \triangleq \frac{v_y\left(\frac{t}{\sqrt{Q}}\right)}{Q}, \qquad \hat{v}_z(t) \triangleq \frac{v_z\left(\frac{t}{\sqrt{Q}}\right)}{Q} \tag{18a}$$

$$\hat{A}_y(t) \triangleq \frac{A_y\left(\frac{t}{\sqrt{Q}}\right)}{Q}, \qquad \hat{A}_z(t) \triangleq \frac{A_z\left(\frac{t}{\sqrt{Q}}\right)}{Q} \tag{18b}$$

$$\hat{V}(t) \triangleq \frac{V\left(\frac{t}{\sqrt{Q}}\right)}{V_M}, \qquad \hat{r}(t) \triangleq \frac{r\left(\frac{t}{\sqrt{Q}}\right)}{V_M}, \qquad \hat{W}(t) \triangleq \frac{W\left(\frac{t}{\sqrt{Q}}\right)}{V_M}, \qquad \hat{q}(t) \triangleq \frac{q\left(\frac{t}{\sqrt{Q}}\right)}{V_M} \tag{18c}$$

respectively. Through simple calculation using the definitions of Q, H_a, and H_b, we then can show that the time-scaled transformation in (18) transforms the almost-linear system in (17) to

$$\text{yaw channel} \quad \begin{cases} \dot{\hat{V}} = \sqrt{\frac{\rho}{2}}\hat{v}_y \\ \dot{\hat{r}} = -\sqrt{\frac{\rho}{2}}H_a(\hat{V},\hat{W}) - \sqrt{\frac{\rho}{2}}h_v\hat{v}_y - \sqrt{\frac{2}{\rho}}h_v\hat{r} \\ \hat{A}_y = \hat{v}_y + \frac{2}{\rho}\hat{r} \end{cases} \tag{19a}$$

$$\text{pitch channel} \quad \begin{cases} \dot{\hat{W}} = \sqrt{\frac{\rho}{2}}\hat{v}_z \\ \dot{\hat{q}} = \sqrt{\frac{\rho}{2}}H_b(\hat{V},\hat{W}) + \sqrt{\frac{\rho}{2}}h_v\hat{v}_z - \sqrt{\frac{2}{\rho}}h_v\hat{q} \\ \hat{A}_z = \hat{v}_z - \frac{2}{\rho}\hat{q} \end{cases} \tag{19b}$$

The above new system depends not any more on V_M but still on ρ. Fortunately, it is possible to make the I/O dynamic characteristics of the new system in (19) almost independent of air density. To this aim, we propose the following class of dynamic compensators:

$$\mathcal{L}[\hat{v}_y(t)] = G_o(s)\{G_f(s)(\mathcal{L}[\hat{A}_y(t)] - \mathcal{L}[\hat{A}^c_y(t)]) + \mathcal{L}[\hat{V}(t)]\} \tag{20a}$$

$$\mathcal{L}[\hat{v}_z(t)] = G_o(s)\{G_f(s)(\mathcal{L}[\hat{A}_z(t)] - \mathcal{L}[\hat{A}^c_z(t)]) + \mathcal{L}[\hat{W}(t)]\} \tag{20b}$$

where $G_o(s)$ and $G_f(s)$ are the real rational functions of s given by

$$G_o(s) \triangleq \frac{\sqrt{\frac{2}{\rho}}s^2G(s)}{k_f + (k_fs+1)sG(s)}, \qquad G_f(s) \triangleq \frac{k_f\left(\sqrt{\frac{\rho}{2}}s + h_v\right)}{s}, \qquad k_f \triangleq -\lim_{s\to 0} sG(s). \tag{21}$$

Since the pitch and yaw channels are symmetric, we choose the dynamic compensators for both channels to be identical. And, $G(s)$ is a real rational function of s, which will be specified soon.

Before specifying the real rational function $G(s)$ which appears in (21), we show that the closed-loop system consisting of the new system in (19) and the dynamic compensator in (20) and (21) can be represented in the form shown in Fig. 1. To do this, we first define $\hat{u}_a$ and $\hat{u}_b$ as follows:

$$\hat{u}_a(t) \triangleq \hat{H}_a(\hat{V}(t),\hat{W}(t)), \qquad \hat{u}_b(t) \triangleq \hat{H}_b(\hat{V}(t),\hat{W}(t)). \tag{22}$$

Simple calculation using (19) and (22) then yields

$$\mathcal{L}[\hat{A}_y(t)] = \frac{s^2\mathcal{L}[\hat{V}(t)] - \mathcal{L}[\hat{u}_a(t)]}{\sqrt{\frac{\rho}{2}}s + h_v} \tag{23a}$$

$$\mathcal{L}[\hat{A}_z(t)] = \frac{s^2\mathcal{L}[\hat{W}(t)] - \mathcal{L}[\hat{u}_b(t)]}{\sqrt{\frac{\rho}{2}}s + h_v}. \tag{23b}$$

Next, we solve (20) for $\mathcal{L}[\hat{V}(t)]$ and $\mathcal{L}[\hat{W}(t)]$ by using the first equations of (19a) and (19b), respectively. Substituting (21) into the resulting equations, we then have

$$\mathcal{L}[\hat{V}(t)] = \frac{G(s)\left(\sqrt{\frac{\rho}{2}}s + h_v\right)}{1 + s^2G(s)}\mathcal{L}[\hat{A}_y(t) - \hat{A}^c_y(t)] \tag{24a}$$

$$\mathcal{L}[\hat{W}(t)] = \frac{G(s)\left(\sqrt{\frac{\rho}{2}}s + h_v\right)}{1 + s^2G(s)}\mathcal{L}[\hat{A}_z(t) - \hat{A}^c_z(t)]. \tag{24b}$$

By this with (23), we also have

$$\mathcal{L}[\hat{V}(t)] = -G(s)\left\{\left(\sqrt{\frac{\rho}{2}}s + h_v\right)\mathcal{L}[\hat{A}^c_y(t)] + \mathcal{L}[\hat{u}_a(t)]\right\} \tag{25a}$$

$$\mathcal{L}[\hat{W}(t)] = -G(s)\left\{\left(\sqrt{\frac{\rho}{2}}s + h_v\right)\mathcal{L}[\hat{A}^c_z(t)] + \mathcal{L}[\hat{u}_b(t)]\right\}. \tag{25b}$$

Finally, define the new variables $\hat{A}^c_{yn}$, $\hat{A}^c_{zn}$, $\hat{A}_{yn}$, and $\hat{A}_{zn}$ by

$$\hat{A}^c_{yn} \triangleq \frac{1}{h_v}\sqrt{\frac{\rho}{2}}\dot{\hat{A}}^c_y + \hat{A}^c_y, \qquad \hat{A}_{yn} \triangleq \frac{1}{h_v}\sqrt{\frac{\rho}{2}}\dot{\hat{A}}_y + \hat{A}_y \tag{26a}$$

$$\hat{A}^c_{zn} \triangleq \frac{1}{h_v}\sqrt{\frac{\rho}{2}}\dot{\hat{A}}^c_z + \hat{A}^c_z, \qquad \hat{A}_{zn} \triangleq \frac{1}{h_v}\sqrt{\frac{\rho}{2}}\dot{\hat{A}}_z + \hat{A}_z. \tag{26b}$$

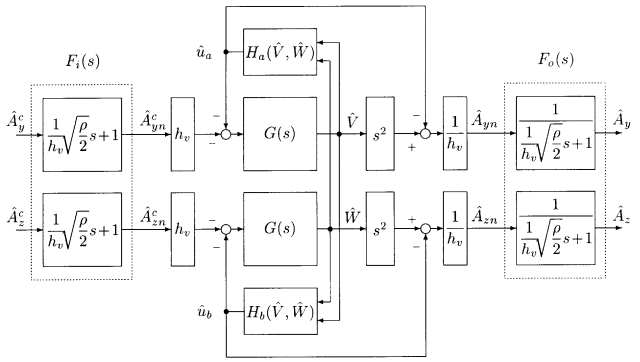

Fig. 1. Equivalent representation of normalized system.

Now, it is easy to see from (22), (23), (25), and (26) that the system in Fig. 1 is equivalent to the closed-loop system given by (19)–(21).

Note from Fig. 1 that the I/O dynamic characteristics from $\hat{A}_n^c \triangleq (\hat{A}_{yn}^c, \hat{A}_{zn}^c)$ to $\hat{A}_n \triangleq (\hat{A}_{yn}, \hat{A}_{zn})$ are independent of air density. On the other hand, $F_i(s)$ and $F_o(s)$ depend on air density but are reciprocal to each other. From this context, we can expect naturally that the I/O dynamic characteristics of the system in Fig. 1 tend to be insensitive with respect to variation in air density. The practical example discussed in Section V supports this expectation well. It also should be clear that when H_a and H_b are linear functions of $\hat{V}$ and $\hat{W}$, the I/O map of the system in Fig. 1 becomes completely independent of air density. From now on, the closed-loop system given by (19)–(21) will be called "normalized system for STT missiles". Our normalized system can greatly simplify the autopilot design procedure. In order to design an autopilot satisfying all given specifications, we do not have to consider simultaneously the family of nonlinear systems indexed by V_M and ρ but only our normalized system that is completely independent of V_M and almost independent of ρ. Later, we discuss this point further.

Now, we are in the order to specify the real rational function $G(s)$ which $G_o(s)$ in (21) contains as a free parameter. To do so, we need to define the set S_r of proper transfer functions as follows.

DEFINITION 1 $G(s) \in S_r$ if and only if

a) $G(s)$ has only one pole at the origin,

b) $G_k(s) \triangleq (1 + (k_1 + k_3)G(s))/(1 + (k_2 - k_3)G(s))$ is strictly positive real, where k_1, k_2, k_3 are the constants satisfying (8).

The condition a) in Definition 1 is required to assure that there exists no steady-state error for constant acceleration commands even in the presence of modeling errors and that k_f in (21) is well defined. On the other hand, the condition b) in Definition 1 along with the sector condition in (8) allows for the direct application of the well-known *Multivariable Circle Criterion* [16] to our normalized system, that is, the closed-loop system given by (19)–(21).

The following theorem shows that any $G(s) \in S_r$ can provide successful set-point tracking for our normalized system. The set S_η defined below specifies the range of admissible constant acceleration commands for which the equilibrium of the normalized system is well defined

$$S_\eta \triangleq \{(\hat{\eta}_y, \hat{\eta}_z) \in \Re^2 : \exists (\hat{V}^*, \hat{W}^*) \in S_{VW} \text{ such that } H_a(\hat{V}^*, \hat{W}^*) = -h_v\hat{\eta}_y,\ H_b(\hat{V}^*, \hat{W}^*) = -h_v\hat{\eta}_z\}.$$

THEOREM 1 *Let the acceleration commands $\hat{A}_y^c$, $\hat{A}_z^c$ to the normalized system, that is, the closed-loop system given by* (19)–(21) *be constant such that*

$$\hat{A}_y^c(t) = \hat{\eta}_y, \qquad \hat{A}_z^c(t) = \hat{\eta}_z, \qquad t \geq 0, \tag{27a}$$

$$(\hat{\eta}_y, \hat{\eta}_z) \in S_\eta. \tag{27b}$$

Then, $G(s) \in S_r$ guarantees that

$$\hat{A}_y(t) \to \hat{\eta}_y, \qquad \hat{A}_z(t) \to \hat{\eta}_z \qquad as \quad t \to \infty. \tag{28}$$

PROOF Suppose that our normalized system is in steady state. Let $\hat{V}^*$, $\hat{W}^*$, $\hat{v}_y^*$, $\hat{v}_z^*$, $\hat{A}_y^*$, and $\hat{A}_z^*$ be the equilibria of $\hat{V}$, $\hat{W}$, $\hat{v}_y$, $\hat{v}_z$, $\hat{A}_y$, and $\hat{A}_z$, respectively. Then, it is clear from (21) and b) of Definition 1 that $G_o(s)G_f(s)$ has one pole at the origin while $G_o(s)$ has no pole at the origin. This with (20) implies that

$$\hat{A}_y^* = \hat{\eta}_y, \qquad \hat{A}_z^* = \hat{\eta}_z. \tag{29}$$

By (19), we also have

$$\hat{v}_y^* = \hat{v}_z^* = 0. \tag{30}$$

As the consequence of (29) and (30), we must have

$$H_a(\hat{V}^*, \hat{W}^*) = -h_v\hat{\eta}_y, \qquad H_b(\hat{V}^*, \hat{W}^*) = -h_v\hat{\eta}_z. \tag{31}$$

Note that (27b) assures the existence of $\hat{V}^*$ and $\hat{W}^*$ satisfying (31). Hence, we have shown that the closed-loop system given by (19)–(21) has the equilibrium point satisfying (29)–(31).

In order to prove absolute stability of the equilibrium point, we shift the equilibrium point to the origin. To do so, we define some new state variables as follows:

$$\begin{aligned} &\tilde{V} \triangleq \hat{V} - \hat{V}^*, \qquad \tilde{A}_y \triangleq \hat{A}_y - \hat{A}_y^*, \\ &\tilde{u}_a \triangleq \tilde{H}_a(\tilde{V}, \tilde{W}, \hat{V}^*, \hat{W}^*) \\ &\tilde{W} \triangleq \hat{W} - \hat{W}^*, \qquad \tilde{A}_z \triangleq \hat{A}_z - \hat{A}_z^* \\ &\tilde{u}_b \triangleq \tilde{H}_b(\tilde{V}, \tilde{W}, \hat{V}^*, \hat{W}^*) \end{aligned} \tag{32}$$

where $\tilde{H}_a$ and $\tilde{H}_b$ have been defined in (7). Through direct calculation using (29)–(32) along with (23) and

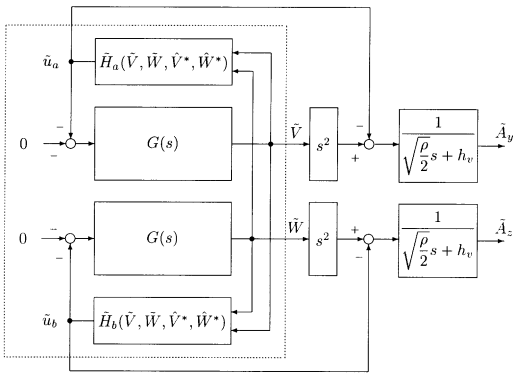

Fig. 2. Equivalent representation of normalized system in case of constant acceleration commands.

(25), we then can convert the closed-loop system given by (19)–(21) to the following system with no input and with the equilibrium point at the origin:

$$\begin{bmatrix}\mathcal{L}[\tilde{V}(t)]\\ \mathcal{L}[\tilde{W}(t)]\end{bmatrix} = \begin{bmatrix}G(s) & 0\\ 0 & G(s)\end{bmatrix}\begin{bmatrix}\mathcal{L}[\tilde{u}_a(t)]\\ \mathcal{L}[\tilde{u}_b(t)]\end{bmatrix} \tag{33a}$$

$$\begin{bmatrix}\tilde{u}_a(t)\\ \tilde{u}_b(t)\end{bmatrix} = -\begin{bmatrix}\tilde{H}_a(\tilde{V}(t),\tilde{W}(t),\hat{V}^*,\hat{W}^*)\\ \tilde{H}_b(\tilde{V}(t),\tilde{W}(t),\hat{V}^*,\hat{W}^*)\end{bmatrix} \tag{33b}$$

$$\begin{bmatrix}\mathcal{L}[\tilde{A}_y(t)]\\ \mathcal{L}[\tilde{A}_z(t)]\end{bmatrix} = \frac{1}{\sqrt{\frac{\rho}{2}}s+h_v}\begin{bmatrix}s^2\mathcal{L}[\tilde{V}(t)]-\mathcal{L}[\tilde{u}_a(t)]\\ s^2\mathcal{L}[\tilde{W}(t)]-\mathcal{L}[\tilde{u}_b(t)]\end{bmatrix}. \tag{33c}$$

The block diagram representation of the above shifted system is given in Fig. 2, and alternatively, can be obtained by applying an appropriate loop transformation to the equivalent representation of the normalized system in Fig. 1.

Note the feedback system given by (33a) and (33b) or the one in the dashed box of Fig. 2 contains a linear time-invariant system in feedfoward path and a memoryless nonlinearity in feedback path. On the other hand, Lemma 1 implies that there exist two 2×2 diagonal matrices $K_{\max}(=(k_1+k_3)I)$, $K_{\min}(=(k_2-k_3)I)$ such that $K_{\max}-K_{\min}>0$ and

$$\left\{\begin{bmatrix}\tilde{H}_a\\ \tilde{H}_b\end{bmatrix}-K_{\max}\begin{bmatrix}\tilde{V}\\ \tilde{W}\end{bmatrix}\right\}^{\mathrm{T}}\left\{\begin{bmatrix}\tilde{H}_a\\ \tilde{H}_b\end{bmatrix}-K_{\min}\begin{bmatrix}\tilde{V}\\ \tilde{W}\end{bmatrix}\right\}\le 0 \tag{34}$$

for all $(\tilde{V},\tilde{W})\in\Re^2$ satisfying $(\tilde{V}+\hat{V}^*,\tilde{W}+\hat{W}^*)\in S_{VW}$. By this and Definition 1, we now see that the feedback system in the dashed box of Fig. 2 satisfies all hypotheses of the well-known *Multivariable Circle Criterion Theorem* [16] and hence is absolutely stable. In other words,

$$\tilde{u}_a,\tilde{u}_b,\tilde{V},\tilde{W}\to 0,\qquad \text{as}\quad t\to\infty. \tag{35}$$

By (29), (32), and (33c), this then implies (28). □

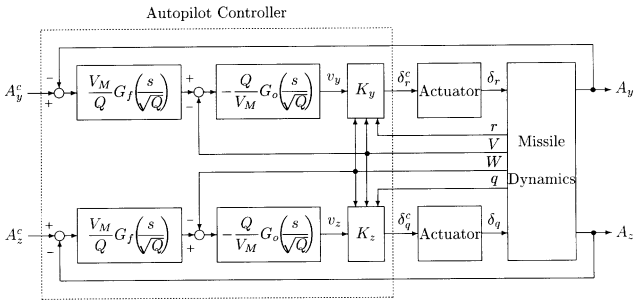

Fig. 3. System configuration of proposed autopilot.

Now, we return to our original problem, that is, design of a high performance autopilot for STT missiles. Note that there are still infinitely many $G(s)$ satisfying the conditions of Definition 1 or stabilizing our normalized system with zero steady-state error. As will be seen soon, a specific choice of $G(s)$ from the set S_r depends on other specifications of autopilot performance such as settling time and overshoot. Suppose for the time being that $G(s)$ is chosen appropriately from the set S_r. Then, we choose the new inputs v_y, v_z of the almost-linear system in (17) by

$$\mathcal{L}[v_y(t)] = \frac{Q}{V_M}G_o\left(\frac{s}{\sqrt{Q}}\right)\times\left\{\frac{V_M}{Q}G_f\left(\frac{s}{\sqrt{Q}}\right)(\mathcal{L}[A_y(t)]-\mathcal{L}[A_y^c(t)])+\mathcal{L}[V(t)]\right\} \tag{36a}$$

$$\mathcal{L}[v_z(t)] = \frac{Q}{V_M}G_o\left(\frac{s}{\sqrt{Q}}\right)\times\left\{\frac{V_M}{Q}G_f\left(\frac{s}{\sqrt{Q}}\right)\left(\mathcal{L}[A_z(t)]-\mathcal{L}[A_z^c(t)]\right)+\mathcal{L}[W(t)]\right\} \tag{36b}$$

respectively, where $G_o(s)$ and $G_f(s)$ are given in (21). In turn, our autopilot controller consists of the partial-linearizing controller in (16) and the dynamic compensator in (21), (36) with $G(s)\in S_r$. The system configuration of our autopilot is described in Fig. 3.

Now, it is easy to show using a well-known property of Laplace transformation that the time-scaled transformation of the input and the output like (18a) and (18b) converts the dynamic compensator in (36) to that in (20). On the other hand, we have seen that the time-scaled transformation in (18) takes the almost-linear system in (17) to the form in (19), while the partial-linearizing controller in (16) takes the original missile model in (2) to the almost-linear system in (17). In conclusion, the closed-loop system given by (2), (16), (21), and (36) is converted through the time-scaled transformation in (18) to the normalized system mentioned earlier. Hence, the following result on the performance of

our autopilot controller naturally follows from this fact along with Theorem 1.

THEOREM 2 *The dynamic behavior of the closed-loop system consisting of the missile model in* (2) *and the autopilot controller given by* (16) *and* (36) *is related in the following manner to that of the normalized system. Suppose that* (18c) *holds for* $t = 0$ *and*

$$\hat{A}_y^c(t) = \frac{A_y^c\left(\frac{t}{\sqrt{Q}}\right)}{Q}, \qquad \hat{A}_z^c(t) = \frac{A_z^c\left(\frac{t}{\sqrt{Q}}\right)}{Q}, \quad t \geq 0. \tag{37}$$

Then, (18b) *holds for all* $t \geq 0$.

According to Theorem 1 and Theorem 2, our autopilot given by (16), (21), and (36) with $G(s) \in S_r$ can provide successful set-point tracking for STT missiles. That is, it guarantees that

$$A_y(t) \to \eta_y, \qquad A_z(t) \to \eta_z, \qquad \text{as} \quad t \to \infty \tag{38}$$

when the acceleration commands are constant such that

$$A_y^c(t) = \eta_y, \qquad A_z^c(t) = \eta_z, \quad t \geq 0 \tag{39a}$$

$$(\eta_y/Q, \eta_z/Q) \in S_\eta. \tag{39b}$$

Based on this fact, we now describe at some length our autopilot design method. For an instance, suppose that we want to choose $G(s) \in S_r$ such that, in any flight condition over $I_{V_M} \times I_\rho$, the acceleration response of our autopilot to any step command carries no steady-state error and has a settling time less than T_s.

Then, we first choose a positive constant $\hat{T}_s$ such that

$$\hat{T}_s \leq T_s \min_{V_M \in I_{V_M}, \rho \in I_\rho} \sqrt{Q} = T_s \sqrt{\frac{\rho_{\min} |V_{M\min}|^2}{2}}. \tag{40}$$

Next, we choose an appropriate $G(s) \in S_r$ such that the acceleration response of the normalized system with $\rho = \rho_{\min}$ to any step command has a settling time less than $\hat{T}_s$. In fact, we can fix ρ at any other value in I_ρ than $\rho_{\min}$ since the I/O dynamic characteristics of the normalized system are almost independent of ρ, as explained earlier. This is particularly true when $\hat{T}_s \gg h_v \sqrt{2/\rho}$ since $F_i(s)$ and $F_o(s)$ are very fast compared with the desired bandwidth of the normalized system. Then, determine $G_o(s)$ and $G_f(s)$ by (21). Finally, Theorem 1 and 2 assure that our autopilot controller given by (16) and (36) is the desired one.

Notice from Definition 1 that $G(s)$ can be chosen regardless of its relative degree. However, the relative degree of $G(s)$ need be chosen at least three for good transient response. Otherwise, the effect of the time-derivatives of $\hat{A}_y^c$ and $\hat{A}_z^c$ may appear directly and can cause excessive undershoot and overshoot in time responses of $\hat{A}_y$ and $\hat{A}_z$. This can be seen easily from Fig. 1. Unfortunately, a systematic way of determining a desired $G(s)$ is not known presently. Nonetheless, Theorem 1 and 2 help to simplify greatly the gain-scheduling process which is required to obtain robust performance with respect to variations in flight conditions such as V_M and ρ.

Note that our autopilot controller given by (16), (21), and (36) with $G(s) \in S_r$ requires the information of Q, q, r, U, V, W, A_y, and A_z. This information can be acquired from Pitot/static tube, rate gyros, ground tracker, accelerometers, or on-board IMU (inertial measurement unit). Otherwise, we may have to design some estimators. On the other hand, the aerodata are available only with some modeling errors. Accordingly, the partial-linearizing controllers K_y, K_z determined by using the aerodynamic force data with some uncertainties cannot be exactly the inverses of H_y, H_z, respectively. As the result, (30) may not hold. Even in the presence of the modeling errors which may yield $v_y^* \neq 0$ and $v_z^* \neq 0$, however, our choice of $G_o(s)$ and $G_f(s)$ like (21) assures (29). This is implied by the arguments used in the Proof for Theorem 1. Unfortunately, it seems quite difficult to analyze in a mathematically rigorous way the effect of errors in modeling and sensing on the performance of our autopilot controller. Instead, we show through simulation in the next section that the performance of our autopilot controller is quite robust with respect to errors in modeling and sensing.

V. PRACTICAL EXAMPLE

In this section, we consider a practical example in order to illuminate further the practical use of our autopilot design method presented in the previous sections. We assume that the ranges of total velocity, air density, and control fin deflection are given as follows:

$$\begin{aligned} I_{V_M} &\triangleq [1.5V_S, 3.0V_S], \\ I_\rho &\triangleq [0.4 \text{ kg/m}^3, 1.2 \text{ kg/m}^3] \\ I_\delta &\triangleq [-25^\circ, 25^\circ] \end{aligned} \tag{41}$$

where I_ρ corresponds to the range of altitude from the sea level up to about 10 km.

Some typical aerodata of the short-range surface-to-air STT missile for which we attempt to design an autopilot are plotted graphically in Fig. 4. For readability, we have described H_m and H_z in terms of α, β, ϕ, and M. Fig. 4(a) shows that H_m is highly nonlinear about α. In particular, the derivative of H_m with respect to α changes its sign at about $\pm 5^\circ$ and $\pm 10^\circ$. On the other hand, we see from Fig. 4(b) that H_z is invertible for δ_q and hence that A7 is satisfied. Therefore, we can find the functions K_y and K_z in look-up table form, which satisfy (15). By

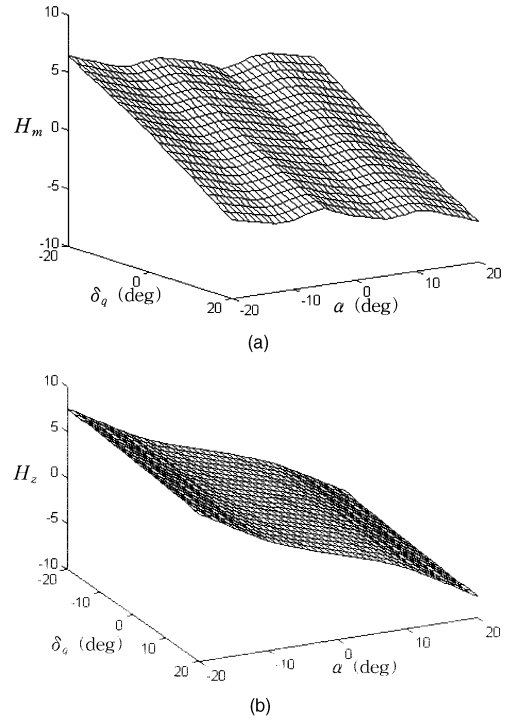

Fig. 4. 3D graphic representation of H_m and H_z ($V_M = 2.5V_S$, $\phi = 45°$).

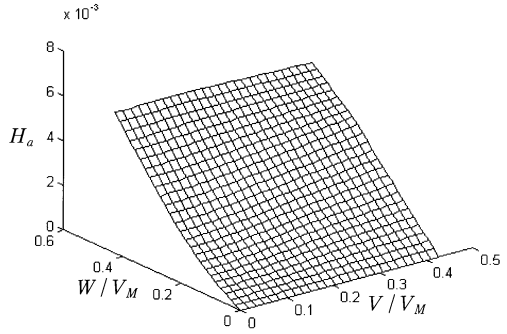

Fig. 5. 3D graphic representation of H_a.

using (14), we also can determine the functions H_a and H_b in look-up table form. As was mentioned in Section III, the functions H_a, H_b depend not only on V/V_M, W/V_M but also on V_M, δ_r, δ_q. However, our computation result has shown that the variations of H_a and H_b due to V_M, δ_r, δ_q are less than 6.5% in the ranges specified in (41) and hence are neglected in the design process for our autopilot controller. The 3D graphic representation of the function H_a given in Fig. 5 reveals that H_a is strictly increasing in V/V_M. Hence, the assumption A8 is well justified. In fact, it can be shown that H_a in Fig. 5 satisfies (9) with

$$k_1 = 0.025, \qquad k_2 = 0.0062, \qquad k_3 = 0.0026. \tag{42}$$

Now, we illustrate our design procedure step by step. We want to design an autopilot which can track

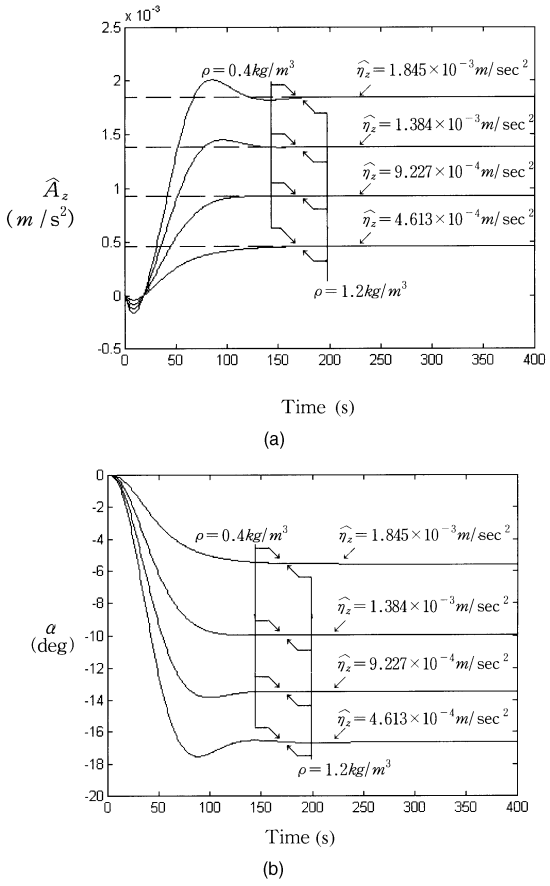

Fig. 6. Step responses of normalized system with $G(s)$ in (43) ($\hat{\eta}_y = 0$).

step acceleration commands with zero steady-state error, overshoot less than 5%, undershoot less than 10%, and settling time shorter than 0.3 s over all the ranges of V_M and ρ given in (41). Then, we can choose $\hat{T}_s = 68$ s by using (40) and (41). According to Theorem 1 and 2, what we need to do is simply to search for a $G(s) \in S_r$ that can have the system in Fig. 1 track step acceleration commands with zero steady-state error, overshoot less than 5%, undershoot less than 10%, and settling time 68 s. By trial and error methods, we have found that the following $G(s)$ meets these performance specifications:

$$G(s) = \frac{1}{s(40s^2 + 6s + 0.4)} \tag{43}$$

as can be seen from the simulation results in Fig. 6. Also, it is easy to check that $G(s)$ in (43) satisfies all conditions in Definition 1 and hence that $G(s) \in S_r$. Note that we have chosen the relative degree of $G(s)$ to be three for good transient performance. On the other hand, Fig. 6 shows that the step responses of our normalized system with $G(s)$ in (43) for the case of $\rho = 0.4$ kg/m^3 are hard to be distinguished from those for the case of $\rho = 1.2$ kg/m^3. Hence, our simulation results demonstrate that the I/O dynamic

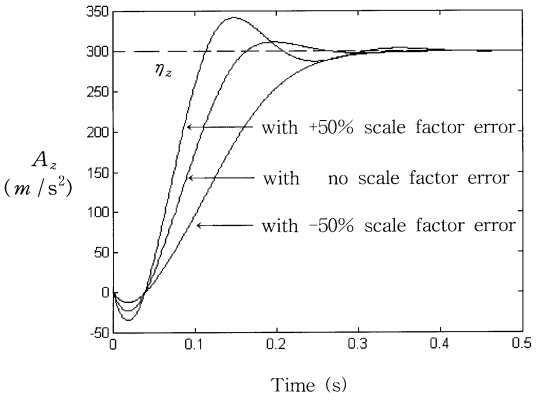

Fig. 7. Step responses of closed-loop system consisting of (2), (16), (36), (44) in presence of scale factor error in H_z ($V_M = 2.5V_S$, $\eta_y = 0$).

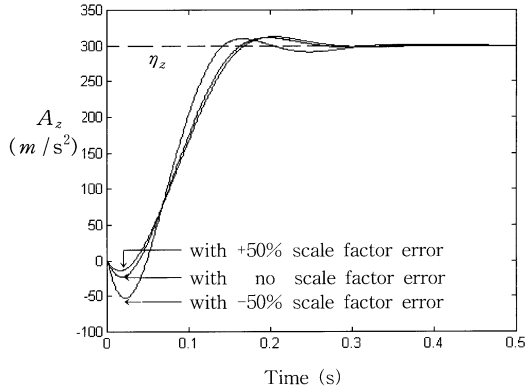

Fig. 8. Step responses of closed-loop system consisting of (2), (16), (36), (44) in presence of scale factor error in H_m ($V_M = 2.5V_S$, $\eta_y = 0$).

characteristics of the normalized system are not only independent of V_M but also almost independent of ρ.

Once we choose $G(s)$ so as to meet the desired performance specifications, we can determine $G_o(s)$ and $G_f(s)$ immediately by using (21) as follows:

$$G_f(s) = -\frac{1}{0.4}\left(\sqrt{\frac{\rho}{2}} + \frac{1.5}{s}\right), \qquad G_o(s) = -\frac{0.4\sqrt{\frac{2}{\rho}}}{40s+7}. \tag{44}$$

It should be noted from Theorem 2 that the step responses of the closed-loop system consisting of (2), (16), (36), and (44) in a flight condition $(V_M, \rho) \in I_{V_M} \times I_\rho$ are identically the same as those in Fig. 6 with the scales of 1 s to $1/\sqrt{Q}$ s and 1 m/s^2 to Q m/s^2. For a numerical example, consider the case of $\rho = 0.6$ and $V_M = 2.5V_S$. Then, the step response of our autopilot for $\eta_y = 400$ m/s^2 corresponds to that for $\hat{\eta}_y = 1.85 \times 10^{-3}$ m/s^2 in Fig. 6. And, the scales of the x- and y-axes in Fig. 6 should be multiplied, respectively, by 2.148×10^{-3} and 2.167×10^5.

On the other hand, Fig. 7 and 8 present the simulation results for the cases when the actual aerodynamic data are largely deviated from those used in the autopilot design. We see from Fig. 7 and 8 that our controller still can provide zero steady-state error and good transient responses even in the presence of large scale factor errors in aerodynamic data. Furthermore, our simulation study has shown that the effect of the estimation errors of V, W, and V_M less than 20% on the dynamic performance of our closed-loop system are not noticeable.

In order to verify the assumption A9, we have considered the following type of actuator dynamics:

$$\tau\dot{\delta}_r = -\delta_r + \delta_r^c \tag{45a}$$

$$\tau\dot{\delta}_q = -\delta_q + \delta_q^c. \tag{45b}$$

Our simulation study has shown that the actuator dynamics with $\tau \leq 0.02$ does not cause any noticeable

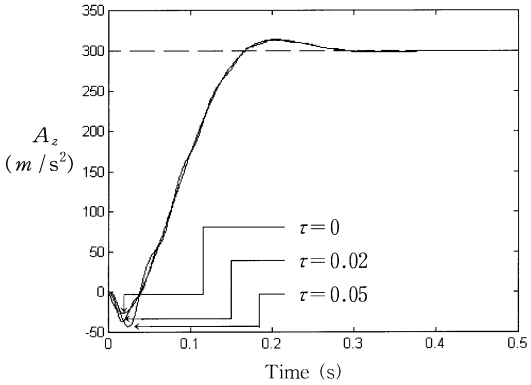

Fig. 9. Effect of actuator dynamics ($V_M = 2.5V_S$, $\phi = 45°$).

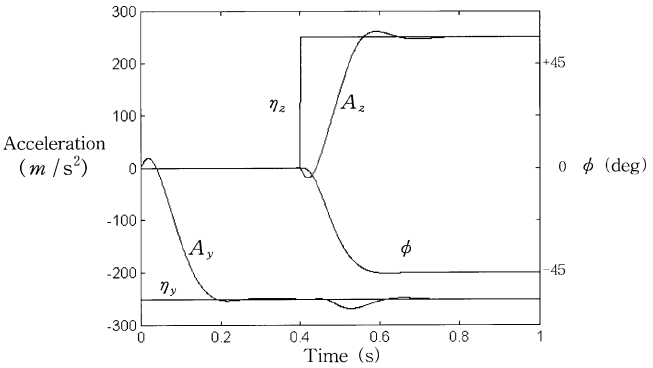

Fig. 10. Effect of fast-varying bank angle ($V_M = 2.5V_S$).

degradation of dynamic performance. Fig. 9 presents the simulation results for three cases: $\tau = 0$, $\tau = 0.02$, and $\tau = 0.05$.

As was mentioned in Section III, the pitch and yaw channels of the missile dynamics are still coupled through the bank angle ϕ even when the roll rate is zero. In order to show that the bank angle can change rapidly and largely in case of high maneuvering, we make step changes from $\eta_y = 0$ to $\eta_y = -250$ m/s^2 at $t = 0$ s and $\eta_z = 0$ to $\eta_y = 250$ m/s^2 at $t = 0.5$ s. Observe from Fig. 10 that the bank angle changes rapidly from 0° to −45°, but our autopilot controller

still provides good set-point tracking performance, although some coupling occurs between pitch and yaw channels. This is because our approach to autopilot design takes the effect of the bank angle into account.

Until now, we have assumed that V_M and ρ are constant. See A2. However, the recent stability analysis on gain-scheduled system [6] or the well-known theoretical results on slow-varying systems [16] suggest that our autopilot controller still will provide good performance if V_M and ρ vary slowly compared with the autopilot dynamics. Finally, we verify this through simulation. To this aim, we make a scenario of flight path as is shown in Fig. 11(a), where V_M and ρ decrease at constant rate, respectively, from Mach 3 to Mach 1.5 and from 1.2 kg/m^3 to 0.4 kg/m^3 in 4 s. Note that along the flight path, Q decreases $\frac{1}{12}$ times in 4 s. In this situation, a series of large step acceleration commands as is shown in Fig. 11(b) is given to our autopilot controller. As the result, the step commands swing the angle of attack through a wide range as can be seen from Fig. 11(c). In Fig. 11(b), we see that all performance specifications are met even in such an ill-conditioned flight situation. Hence, the simulation results in Fig. 11 convince us that our approach to autopilot design provides not only a very simple but also quite effective gain-scheduling procedure for robust performance. It also suggests that our autopilot controller still can give good performance even in flight with the thrust burn in.

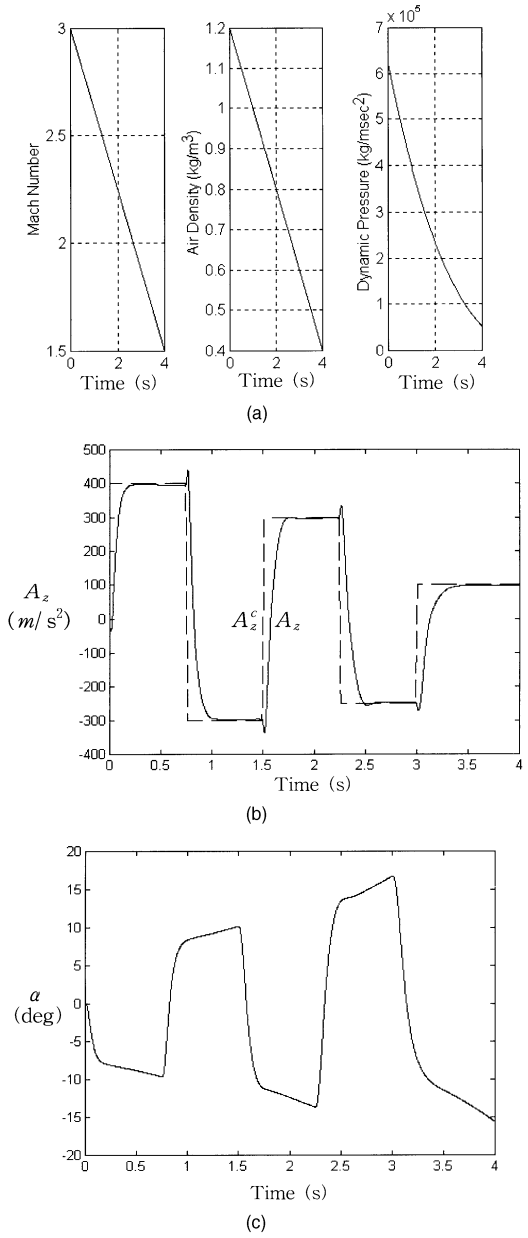

Fig. 11. Step responses of closed-loop system consisting of (2), (16), (36), (44) for sequence of step commands ($A_y^c(t) = 0$ m/s^2). (a) Scenario of flight path (Mach number M, air density ρ, dynamic pressure Q). (b) Acceleration. (c) Angle of attack.

VI. CONCLUSIONS

In this paper, we have proposed a new approach to acceleration control of STT missiles and demonstrated its generality and practical use through stability analysis and simulation. Our autopilot controller may require large memory to store the exact inversions of H_y and H_z in look-up table form. Please see (15). This problem can be resolved easily due to the recent semiconductor production technology. Moreover, our simulation results shows that the effect of imperfect functional inversion on stability and performance is not significant. The highlights in our approach are 1) the very simple gain-scheduling procedure based on the normalized system, and 2) the rigorous stability analysis of our autopilot controller based on the full nonlinear model for STT missiles.

Nonetheless, some important issues still remain untouched. For instance, we have assumed that roll-stabilization is perfect. However, some roll rate is unavoidable in practice and can cause some fluctuation in missile acceleration. In order to reduce further the effect of roll rate on the pitch and yaw channels, we may have to consider other types of dynamic compensators. This issue is directly related to extension of our work to BTT missiles and need be explored more extensively in future. On the other hand, the sampling rate should be chosen carefully in case of digital implementation of our autopilot controller. In fact, our simulation study for the case of the practical example shows that a sampling rate slower than 1 kHz can cause some oscillation in acceleration responses. However, this can be expected since our autopilot is designed to have the settling time less than 0.3 s in any flight condition.

REFERENCES

[1] Blakelock, J. H. (1991)
Automatic Control of Aircraft and Missile.
New York: Wiley, 1991.

[2] Tahk, M., Briggs, M., and Menon, P. K. A. (1988)
Application of a plant inversion via state feedback to missile autopilot design.
In *Proceedings of IEEE Conference on Decision and Control*, Austin, TX, Dec. 1988, 730–735.

[3] Reboulet, C., and Champetier, C. (1984)
A new method for linearizing nonlinear systems: The pseudolinearization.
International Journal of Control, **40**, 4 (Apr. 1984), 631–638.

[4] Nichols, R. A., Reichert, R. T., and Rugh, W. J. (1993)
Gain-scheduling for H-infinity controllers: A flight control example.
IEEE Transactions on Control Systems Technology, **1**, 2 (June 1993), 69–79.

[5] Shamma, J. S., and Cloutier, J. R. (1993)
Gain-scheduled missile autopilot design using linear parameter varying transformation.
Journal of Guidance, Control, and Dynamics, **16**, 2 (1993), 256–263.

[6] Shamma, J. S., and Athans, M. (1990)
Analysis of nonlinear gain-scheduled control systems.
IEEE Transactions on Automatic Control (Aug. 1990), 898–907.

[7] Isidori, A. (1989)
Nonlinear Control System.
Berlin: Springer-Verlag, 1989.

[8] Ha, I. J., and Chong, S. (1992)
Design of a CLOS guidance law via feedback linearization.
IEEE Transactions on Aerospace and Electronic Systems, **28** (Jan. 1992), 51–62.

[9] Meyer, G., Su, R., and Hunt, L. R. (1984)
Application of nonlinear transformations to automatic flight control.
Automatica, **20** (1984), 103–107.

[10] Romano, J. J., and Singh, S. N. (1990)
I-O map inversion, zero dynamics and flight control.
IEEE Transactions on Aerospace and Electronic Systems, **26** (Nov. 1990), 1022–1028.

[11] Huang, J., Lin, C. F., Cloutier, J.R., Evers, J. H., and D'Souza, C. (1992)
Robust feedback linearization approach to autopilot design.
IEEE Conference on Control Application, **1** (1992), 220–225.

[12] Lin, C. F. (1994)
Advanced Control Systems Design.
Englewood Cliffs, NJ: PTR Prentice Hall, 1994.

[13] Marino, R. (1986)
On the largest feedback linearizable subsystems.
Systems and Control Letters, **6** (1986), 345–351.

[14] Respondek, W. (1986)
Partial linearization, decomposition and fibre linear systems.
In *Theory and Application of Nonlinear Control Systems*.
North-Holand, Elsevier, 1986, 137–154.

[15] Morton, B. (1992)
A dynamic inversion control approach for high-mach trajectory tracking.
In *Proceedings of the American Control Conference*, Chicago, IL, June 1992, 1332–1336.

[16] Khalil, H. K. (1992)
Nonlinear Systems.
New York: Macmillan, 1992.

[17] Apostol, T. M. (1974)
Mathematical Analysis.
Reading, MA: Addison-Wesley, 1974.

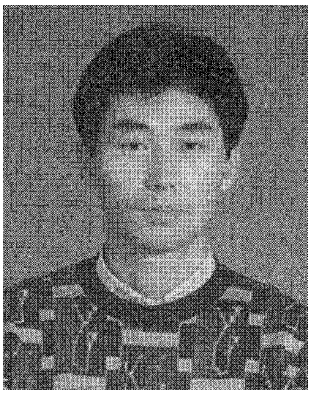

Jae-Hyuk Oh was born in Seoul, Korea, on September 9, 1966. He received the B.S., M.S., and Ph.D. degrees in control and instrumentation engineering from Seoul National University, Seoul, Korea, in 1989, 1991, and 1996, respectively.

He is presently a senior researcher at Automatic Control Research Center, Seoul National University. His current field of interest is nonlinear control theory and its applications to missile guidance and control.

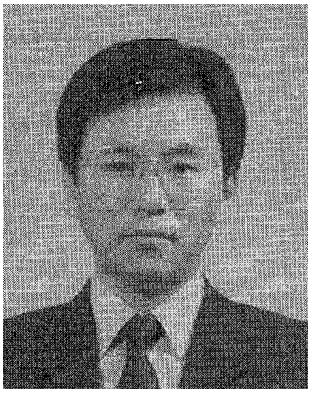

In-Joong Ha received the Ph.D. degree in computer, information, and control engineering (CICE) from the University of Michigan, Ann Arbor, in 1985.

He is presently a Professor in the Department of Control and Instrumentation Engineering, Seoul National University, Seoul, Korea. From 1973 to 1981, he worked in the area of missile guidance and control at the Agency of Defense Development in Korea. From 1982 to 1985, he was a Research Assistant at the Center for Research on Integrated Manufacturing, University of Michigan, AnnArbor. From 1985 to 1986, he was with General Motors Research Laboratories, Troy, MI. His current research interest includes nonlinear control theory and its applications to missiles, electric machines, and high precision servo systems for factory automation and multimedia.

Dr. Ha was the recipient of the 1985 Outstanding Achievement Award in the CICE program.